Animal Nutrition 12 (2023) 236–244

Contents lists available at ScienceDirect

Animal Nutrition

journal homepage: http://www.keaipublishing.com/en/journals/aninu/

Original Research Article

# Point-of-care testing for lysine concentration in swine serum via blue-emissive carbon dot-entrapped microfluidic chip

Chizhu Ding, Xiang Chen, Xiaoyu Chen, Yue Liu, Menglin Xia, Ziyi He, Qinshu Kang, Xianghua Yan*

*State Key Laboratory of Agricultural Microbiology, Hubei Hongshan Laboratory, Frontiers Science Center for Animal Breeding and Sustainable Production, College of Science, College of Animal Sciences and Technology, College of Veterinary Medicine, Huazhong Agricultural University, Wuhan, 430070, China*

ARTICLE INFO

*Article history:*
Received 3 May 2022
Received in revised form
16 June 2022
Accepted 13 August 2022
Available online 27 October 2022

*Keywords:*
Lysine
Swine serum
Carbon dots
Microfluidics
Point-of-care testing

ABSTRACT

Lysine is one of the essential amino acids and plays a vital role in the growth, development and health of pigs. Blood lysine concentration is a direct indication of lysine status; however, current methods can not satisfy the demands for rapid and on-site lysine concentration measurement of swine serum. Here, we developed blue-emissive nitrogen-doped carbon dots as a fluorescence probe for the determination of lysine with high fluorescence quantum yield, stability, sensitivity and specificity. The carbon dots were entrapped within hydrogel microstructures to fabricate microfluidic chips for rapid assay for lysine quantification. We further developed an imaging attachment to integrate the microfluidic chip and a smartphone into a portable point-of-care testing platform. This platform requires only 3 μL sample and has a linear detection range of 25 to 300 μmol/L with a limit of detection less than 16 μmol/L, which covers the normal range of lysine concentration in swine serum. We tested lysine concentration in swine serum using this platform with high accuracy, low sample consumption, and within 3 min. Together, these results may provide a rapid and portable platform for dynamic monitoring of swine lysine status and contribute to precise feed formula modulation with low-protein diet strategy.


## 1. Introduction

Lysine is one of the essential amino acids and the first limiting amino acid in corn-soybean meal based low-protein diets for swine (Wang et al., 2018). Dietary deficiency of lysine will reduce the growth performance, affect the metabolism of other nutrients, impair the immunity and increase the susceptibility to infectious diseases (Ettle and Roth, 2009; Liao et al., 2015; Yin et al., 2018). Nevertheless, excess supplementation of lysine will result in waste and affect the absorption and transport of other amino acids such as arginine and histone (Wu et al., 2000; Yin et al., 2017). Because lysine deficiency or excess has negative impact on swine growth performance and health, and lysine requirement is a dynamic variable that relates to multiple factors, a simple and effective assay for lysine status is needed. The blood free amino acid profile reflects the amino acid profile of the consumed supplement (Regmi et al., 2016) and serum amino acid levels can be used to validate the estimated requirement (Roy et al., 2000; Wiltafsky et al., 2009; Zeng et al., 2013). Hence, dynamic monitoring of serum lysine status helps to apply ideal amino acid pattern to maximize the advantages of low-protein diets and simultaneously reduce the cost of supplemental lysine.

Conventional methods for the quantification of lysine, and more generally, amino acids in biological samples include gas chromatography/mass spectrometry (GC/MS) (Culea et al., 2015), high-performance liquid chromatography (HPLC) (Dai et al., 2014), liquid chromatography–tandem mass spectrometry (LC–MS/MS) (Tu et al., 2012), and nuclear magnetic resonance spectroscopy (NMR) (Armstrong et al., 2012). These methods have disadvantages as they require complex sample pre-treatment, expensive instruments and skilled operators and are time consuming. Rapid methods for the determination of lysine concentration have been developed through the use of lysine probes such as gold nanoparticles (AuNPs) (Zhou et al., 2012), gold nanorods (AuNRs) (Wang

* Corresponding author.
*E-mail address:* xhyan@mail.hzau.edu.cn (X. Yan).
Peer review under responsibility of Chinese Association of Animal Science and Veterinary Medicine.

Production and Hosting by Elsevier on behalf of KeAi

https://doi.org/10.1016/j.aninu.2022.08.017

et al., 2012), graphene quantum dots/gold nanoparticles (GQD/AuNPs) (Chaicham et al., 2019), and $Ag^{+}$ oxidized 3,3′,5,5′-tetramethylbenzidine (TMB) (Xue et al., 2019) for colorimetric assays. However, these metal-based nanosensors generally have the limitations of being expensive or hard to prepare, and high toxicity. Carbon dots (CDs) have received increasing attention as optical sensors, owing to the low cost, low toxicity, high stability, and ease of synthesis and functionalization (Baker and Baker, 2010; Morbioli et al., 2017). Recently, fluorescent CDs have been synthesized for lysine detection (Song et al., 2017; Sharma and Yun, 2020). However, the application of these CDs is still limited by photostability, specificity and detection range.

Currently, point-of-care testing (POCT) is rapidly emerging as an alternative to the traditional laboratory-based testing. A considerable number of POCT devices use microfluidics. A microfluidic chip is a small portable platform that can complete sample pretreatment, mixing and chemical reaction by fluid manipulation in a singular device with increased speed and reduced consumption of samples (Xie et al., 2022). A typical strategy is integrating hydrogel microstructures mixed with probes serving as sensing elements inside the microchannels (Lin et al., 2011; Jang et al., 2012). Due to the rapid development and widespread use of smartphones, more and more POCT devices are developed by using a smartphone as a detector, a data processor and a result display (Liu et al., 2019).

Here we report a smartphone-based POCT platform for the determination of lysine via a blue-emissive carbon dot-entrapped microfluidic chip. The POCT platform was applied to a swine serum sample to demonstrate its performance.

## 2. Materials and methods

### 2.1. Animal ethics statement

The experiment protocol was approved by the Animal Care and Use Committee of Huazhong Agricultural University, Wuhan, China (approval number: HZAUSW-2002-0009).

### 2.2. Materials

Tetraethylene glycol and acrylic acid were purchased from Adamas-Beta Ltd. (Shanghai, China). Zinc chloride, methanol, diethyl ether, sodium chloride and potassium chloride were purchased from Sinopharm Chemical Reagent Co., Ltd. (Shanghai, China). Poly (ethylene glycol) diacrylate (PEG-DA), photoinitiator 2-hydroxy-2-methylpropiophenone (HOMPP), and lysine were purchased from Sigma-Aldrich (St. Louis, MO, USA). Polydimethylsiloxane (PDMS) prepolymer was obtained from Dow Corning (Midland, MI, USA). All the other reagents were purchased from Aladdin Chemistry Co. Ltd. (Shanghai, China). All the chemicals were analytical grade. Millipore water was used to prepare all solutions. Swine serum samples (three-way hybrid pig, 20 d) were obtained from College of Animal Sciences and Technology, Huazhong Agricultural University.

### 2.3. Instruments

The fluorescence spectra were obtained using a spectrofluorophotometer (Shimadzu RF-6000, Japan). The ultraviolet−visible (UV−vis) spectra were obtained using a UV−vis spectrophotometer (Shimadzu UV-1800, Japan). The Fourier transform infrared (FTIR) spectra were obtained using a FTIR spectrometer (Thermo Scientific Nicolet iS50, USA). The morphology and particle size of the nitrogen-doped carbon dots (N-CDs) were performed on a field-emission transmission electron microscope (TEM; FEI Tecnai G2 F20 S-TWIN TEM, USA). X-ray power diffraction (XRD) pattern was obtained using an X-ray diffractometer (Bruker D8 Advance, Germany) with Cu-Kα radiation ($\lambda$ = 1.5418 Å). X-ray photoelectron spectroscopy (XPS) was performed using an XPS spectrometer (Thermo Scientific Escalab 250Xi, USA) equipped with an Al Kα X-Ray source. Fluorescence images were obtained using an inverted fluorescence microscope (Nikon Eclipse Ti2, Japan) with a halogen lamp. The concentrations of free amino acids in swine serum samples were measured using an automatic amino acid analyzer (Hitachi L-8900, Japan).

### 2.4. Synthesis of N-CDs

A 25-mL one-necked round bottom flask containing tetraethylene glycol solution (5 mL) was charged with $ZnCl_2$ (340 mg, 2.5 mmol), 2,3-diaminopyridine (55 mg, 0.5 mmol) and acrylic acid (220 mg, 3.0 mmol). The resulting mixture was first stirred at 100 °C for 1 h under $N_2$ atmosphere, and then the reaction was kept with magnetic stirring at 210 °C for another 4 h. After cooling, the crude product was suspended in methanol (40 mL), and the supernatant was collected by centrifugation. The solution was subjected to vacuum concentration to a volume of about 20 mL, and diethyl ether (50 mL) was added to precipitate the product. This precipitation step was repeated twice to remove the residual $ZnCl_2$ completely, and the obtained black solid was dried under vacuum at 40 °C to obtain the final N-CD product.

### 2.5. Detection of lysine using N-CDs

For the detection of lysine, 100 μL of lysine solutions with different concentrations were separately added into 2 mL phosphate buffer saline (PBS) solution containing N-CDs ($C_{N\text{-}CDs}$ = 0.05 mg/mL, pH = 6.0). Then, the fluorescence emission spectra were recorded. The selectivity of the N-CDs towards lysine was verified by adding various interferences into the N-CDs solution under the same conditions as the detection of lysine. The final concentration of amino acids was 500 μmol/L, except lysine was 200 μmol/L and Gly was 2,000 μmol/L. The concentrations of glutathione (GSH) and glucose were 2,000 and 10,000 μmol/L, respectively. The concentrations of metal ions were 10 μmol/L, except $K^{+}$ and $Na^{+}$ which were 100,000 μmol/L. The selected concentrations of the above potential interfering substances were much higher than their typical concentrations in swine serum. To test the photostability of the N-CDs, the N-CDs solution was under continuous illumination of a 365-nm UV lamp and the fluorescence intensity was measured every 15 min. All experiments were carried out at room temperature.

### 2.6. Fabrication of the microfluidic chip

The mold of the microfluidic chip was designed using SolidWorks software (SolidWorks, USA) and fabricated by 3D printing with PlasCLEAR material (Asiga, Australia) by a digital light processing 3D printer (Asiga MAX X35, Australia). The inner surface of the mold was coated with mineral oil to facilitate stripping. Liquid PDMS prepolymer was poured onto the mold and cured at 65 °C for 4 h. The shaped PDMS part was then peeled off from the mold and the open channels were sealed by bonding the PDMS to a glass slide after surface treatment with air plasma. There were 2 identical channels on each microfluidic chip, and each channel had an inlet and an outlet.

The N-CDs-entrapping hydrogel microstructures inside the channels were fabricated by a photopatterning process (Jang et al., 2012). To prepare the hydrogel precursor solution, 1.0 mL solution composed of PEG-DA and PBS (50%, wt/vol), 200 μL solution of N-CDs (0.1 mg/mL), and 10 μL HOMPP was mixed evenly. The mixture was injected into both the detection and the reference channels in

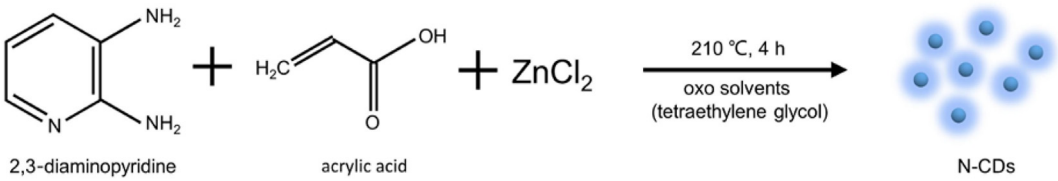


**Fig. 1.** Synthetic routes of nitrogen-doped carbon dots (N-CDs).

the microfluidic chip. The hydrogel was cured by UV exposure for 15 s with a photomask covered on the top of the microfluidic chip. The channels were washed in PBS 3 times. The uncured hydrogel solution was washed away, leaving cured hydrogel microstructures entrapping N-CDs.

### 2.7. Smartphone-based imaging device

To provide a stable illumination and imaging condition and avoid environmental light interference, an imaging box was attached to the smartphone. A light-emitting diode (LED) light source (LED375L, Thorlabs, USA), a condenser lens and a bandpass filter (FGUV11, Thorlabs, USA) were used as an excitation source to illuminate the microfluidic chip from the bottom. The microfluidic chip was put on a slidable stage for input and output from the side of box. A short pass filter (GCC-211005, Daheng Optics, China) was used as an emission filter. The top plate contained a circular aperture for docking the camera of the smartphone. An auxiliary magnification lens (AC064-015-A, Thorlabs, USA) was embedded in the aperture. The imaging box and slidable stage were designed using SolidWorks software and fabricated by a selective laser sintering 3D printer (HP Jet Fusion 4200 3D, USA) using black Polyamide 12 material. The LED, filters and lenses were then assembled in the box. Three smartphones of different brands (Huawei Nova 7 Pro, China; Xiaomi Mi 10S, China and Apple iPhone 11, USA) were used to test the viability of the imaging attachment. The images were taken by the native camera application (Huawei, EMUI 10.1 based on Android 10; Xiaomi, MIUI 12 based on Android 11 and Apple, iOS 7.1.1) and sent to a computer for further processing.

### 2.8. Data analysis

The fluorescent images of the microfluidic chips were taken by a fluorescence microscope or a smartphone with an imaging attachment. To quantify the fluorescence intensity, ImageJ software (NIH, USA) was used to measure the intensity of the region of interest in the image. The captured RGB (red, green, and blue) colored images were converted to 8-bit grayscale images, converting raw data into individual grayscale channel data of light intensity. Changes in the fluorescence intensity were quantified by comparing the mean light intensity ($I$) of the hydrogel region in the detection channel ($I_{det}$) with that of the reference channel ($I_{ref}$) extracted using ImageJ software. In order to further reduce the influence of background light, the mean light intensity of the blank region ($I_{bg}$), i.e., where the light passed only through the PDMS and glass slide, not the hydrogel, was subtracted from both $I_{det}$ and $I_{ref}$. That is, we calculated the value of the relative light intensity $I/I_0 = (I_{det} - I_{bg})/(I_{ref} - I_{bg})$ instead of the value of $I_{det}/I_{ref}$. The relationship between $I/I_0$ obtained by the inverted fluorescence microscope and $C_{Lys}$ was studied. A linear equation with respect to $I/I_0$ versus $C_{Lys}$ was obtained by curve fitting and used as the calibration equation. By using the equation, the lysine concentration of unknown sample could be estimated following the above data processing steps.

## 3. Results

### 3.1. Characterization of N-CDs

To develop a simple method for the determination of lysine, we first synthesized blue-emissive N-CDs as a fluorescence probe via an ionothermal method in organic solvents as described in the Synthesis of the N-CDs section (Fig. 1). The morphology, surface functionalities, structure and chemical composition of the N-CDs were characterized by TEM, FTIR, UV–vis, XRD and XPS. The TEM image (Fig. 2A) revealed that the N-CDs were nearly spherical and well dispersed, with the size ranging from 4 to 8 nm. The high-resolution TEM (HRTEM) image indicated that N-CDs exhibited lattice fringes with a typical interplanar spacing of 0.21 nm, corresponding to the (100) in-plane lattice of graphene (Chen et al., 2016). The histogram of the particle-size distribution was plotted according to the TEM images. The UV–vis absorption spectrum (Fig. 2B) exhibited 2 distinct absorption peaks at 240 and 281 nm, corresponding to the $\pi-\pi^*$ transitions of C=C bonds and the $n-\pi^*$ transitions of C–N bonds (Ju et al., 2014; Long et al., 2018). The characteristic absorption bands in the FTIR spectrum (Fig. 2C) appeared at approximately 3,650 to 3,100 $cm^{-1}$ (O–H and N–H stretching vibrations), 3,000 to 2,800 $cm^{-1}$ (C–H stretching vibration), 1,790 to 1,365 $cm^{-1}$ (C=O and COOH stretching vibration) and 1,080 $cm^{-1}$ (C–O–C stretching vibration). The XRD pattern of N-CDs (Fig. 2D) exhibited a broad peak at 22.6°, corresponding to a $d$-spacing of 3.93 Å, indicating that the N-CDs contain a graphite-like structure (Yuan et al., 2018). The XPS survey (Fig. 2E) revealed that the N-CDs mainly contained 4 elements: C, O, N and Zn. A small amount of Cl element was also observed. The element contents of C, O, N and Zn determined by XPS were 68.05 % (wt/wt), 20.82% (wt/wt), 7.63% (wt/wt) and 3.51% (wt/wt), respectively. The high-resolution C 1s spectrum could be deconvoluted into 5 peaks, at 284.5 eV (C=C/C–C), 285.8 eV (C–N), 286.2 eV (C–OH), 287.1 eV (C=O) and 288.7 eV (COOH). The N 1s spectrum was deconvoluted into 3 peaks, at 398.4 eV (pyridinic N), 399.1 eV (pyrrolic N) and 400.2 eV (graphitic N). The O 1s spectrum was deconvoluted into 2 peaks at 532.0 eV (C=O) and 533.0 eV (C–O).

### 3.2. Optical response of N-CDs for lysine detection

The fluorescence response of the N-CDs for lysine detection was investigated. The optimal excitation wavelength ($\lambda_{ex}$) of N-CDs was 380 nm and the fluorescence peak ($\lambda_{em}$) was 436 nm. The fluorescence emission increased continuously and dramatically with increasing lysine concentration (Fig. 3A). A linear relationship between the fluorescence intensity $I/I_0$ and lysine concentration was achieved ($I/I_0 = 0.00458C_{Lys} + 1.01319$, $R^2 = 0.99693$), where $I$ and $I_0$ were the fluorescence intensities of the N-CDs solution at $\lambda_{em} = 436$ nm after and before adding lysine, respectively. The N-CDs exhibited stronger blue fluorescence intensity in the presence of lysine under UV irradiation (Fig. 3B). The linear detection range was from 5 to 300 μmol/L. The limit of detection (LOD) was calculated to be 1.7 μmol/L based on $3\delta_{blank}$, where $\delta_{blank}$ was the

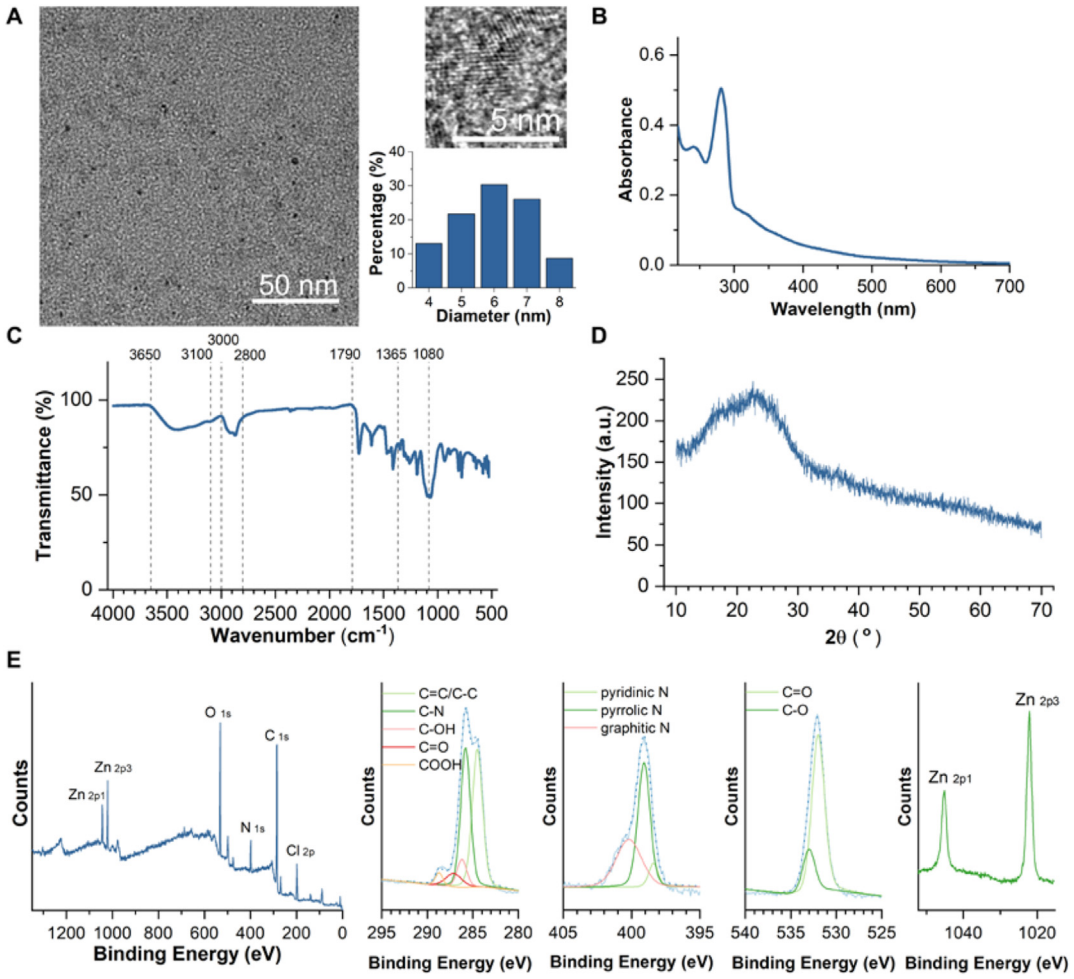


**Fig. 2.** Structural characterization of nitrogen-doped carbon dots (N-CDs). (A) Transmission electron microscopy (TEM), high-resolution TEM (HRTEM) images, and particle-size distribution for N-CDs. (B) Ultraviolet–visible (UV–vis) absorption spectrum. (C) Fourier transform infrared (FTIR) spectrum. (D) X-ray power diffraction (XRD) pattern ($2\theta = 22.6°$, d-spacing = 3.93 Å). (E) X-ray photoelectron spectroscopy (XPS) survey and deconvoluted high-resolution XPS spectra of C 1s, N 1s, O 1s and Zn 2p for N-CDs.

standard deviation of background ($n = 3$). Fig. 3C proved that potential interferers have a negligible effect on lysine detection. The error bars represented the standard deviation of 3 measurements. The fluorescence intensity of the N-CDs was stable under UV irradiation (Fig. 3D).

Moreover, the fluorescence quantum yield (QY) of N-CDs was determined following the relative determination procedure by using quinine sulfate (QY = 0.54 in water) as the standard sample (Würth et al., 2013; Ju et al., 2014). The QY of N-CDs solution was measured to be 24.8% and 34.8% before and after addition of 100 μmol/L lysine with excitation at 380 nm. A high QY lead to the emission of bright blue fluorescence from the N-CDs solution and the significant increase in QY after addition of lysine also confirmed the sensitivity. The above experimental results suggest that the N-CDs can serve as a fluorescence probe for the determination of lysine.

### 3.3. Microfluidic chip-based lysine detection using fluorescence microscope

Then, we fabricated the microfluidic chips following the processing steps described in the fabrication of the microfluidic chip section (Fig. 4). Each microfluidic chip was about 12 mm × 10 mm × 3 mm (length × width × height) containing 2 channels: the detection channel and the reference channel. The main channels were 0.8 × 0.3 mm in width and depth and approximately 6.5 mm long with an inlet and an outlet. The resultant hydrogel microstructures were about 0.73 mm × 0.94 mm in width and length and 0.14 mm in height. The width and height of the microstructures were smaller than that of the channels, leaving enough space for the sample fluid to flow through the channel. The highly cross-linked hydrogels allowed rapid diffusion of the target molecules (Lee et al., 2008). By entrapping the N-CDs, the hydrogel microstructures were fluorescently responsive to lysine.

Images were recorded by an inverted fluorescence microscope immediately after the injection of lysine. As shown in Fig. 5, the fluorescence of the microstructures intensified with increasing lysine. A linear relationship between the relative light intensity, $I/I_0 = (I_{det} - I_{bg})/(I_{ref} - I_{bg})$ and lysine concentration was achieved ($I/I_0 = 0.00471C_{Lys} + 1.01184$, $R^2 = 0.99546$). The LOD was calculated to be 9.7 μmol/L.

### 3.4. Microfluidic chip-based lysine detection using smartphone

As shown in Fig. 6A, the 3D-printed imaging attachment had overall dimensions of 45 mm × 40 mm × 65 mm (length × width × height). The LED, filters, and lenses were then assembled in the box as illustrated in Fig. 6B. The magnification lens used in the

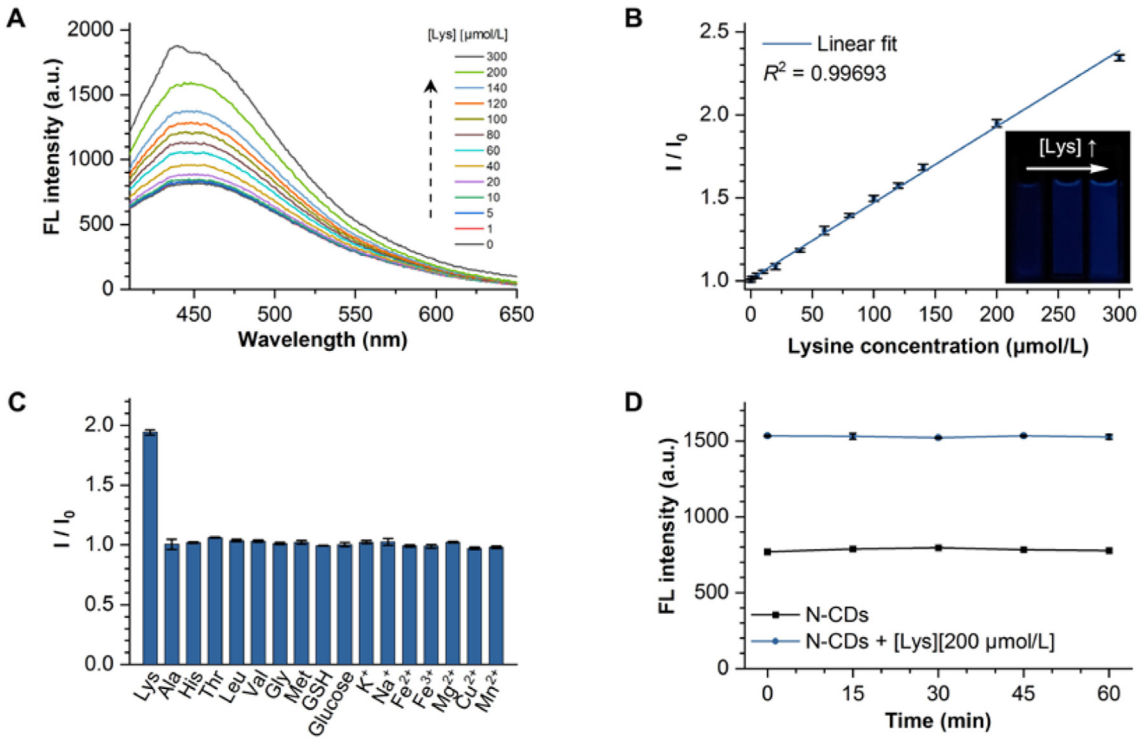


**Fig. 3.** Optical response of nitrogen-doped carbon dots (N-CDs) for lysine detection. (A) Fluorescence emission spectra of N-CDs in the presence of different concentration of lysine ($\lambda_{ex}$ = 380 nm). (B) Linear fitting curve of the relative light intensity ($I/I_0$) versus the concentration of lysine ($\lambda_{em}$ = 436 nm) and image of N-CDs solution under 365 nm UV irradiation. (C) Fluorescence response $I/I_0$ in the presence of different analytes ($\lambda_{ex}$ = 380 nm, $\lambda_{em}$ = 436 nm). (D) Fluorescence stability under UV illumination. FL = fluorescence; a.u. = arbitrary units; GSH = glutathione.

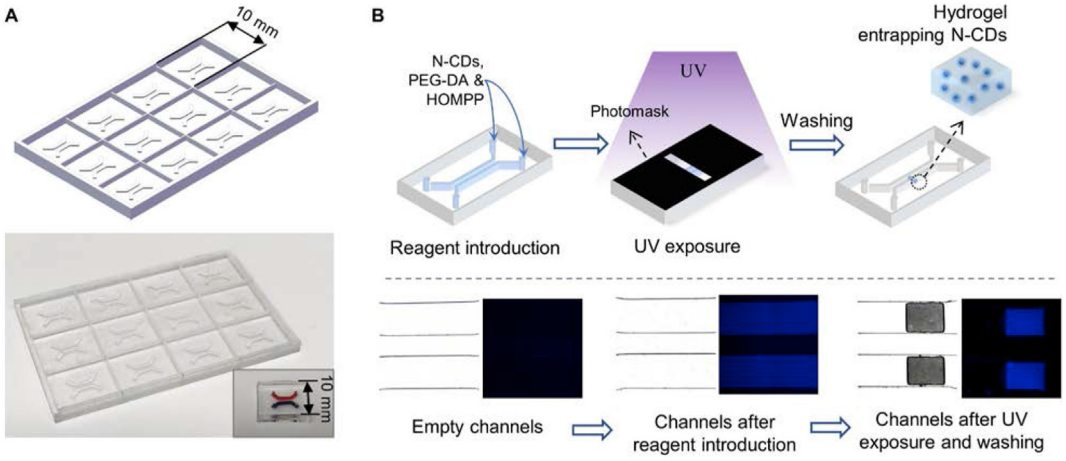


**Fig. 4.** Illustration of fabrication procedures for the microfluidic chip. (A) The 3D design (upper) and photos of the mold and microfluidic chip with red and blue dyes added in the channels for better visual effect (lower). (B) Schematic illustration (upper) and brightfield and fluorescence microscopy images (lower) of fabrication of the nitrogen-doped carbon dots (N-CDs)-entrapping hydrogel microstructures inside the channels. PEG-DA = poly (ethylene glycol) diacrylate; HOMPP = photoinitiator 2-hydroxy-2-methylpropiophenone.

imaging attachment had a focal length, $f$ = 15.0 mm, providing a magnification factor of 16.7 according to the magnification factor formula, $\Gamma = 250/f$ (Chen et al., 2018). The built-in camera of the smartphone also provided enhanced magnification. Three smartphones of different brands and models were used in the experiments. The exposure time varied from 0.2 to 1.1 s. As shown in Fig. 7A, the color of the photographs captured by the microscope and smartphones was slightly different mainly due to the difference in the transmission spectra of the filters, the color temperature settings of the cameras and the exposure time. However, the relative light intensity $I/I_0$ for the same lysine concentration obtained by the 3 smartphones was almost the same. A good linear relationship between $I/I_0$ and $C_{Lys}$ could be achieved by each smartphone (Fig. 7B) and the linear equations derived from the 3 smartphones were nearly identical. By using the linear relationship derived from the Apple smartphone ($I/I_0 = 0.00455C_{Lys} + 1.01985$, $R^2 = 0.99537$) as the calibration equation, each smartphone gave satisfactory measurement results (Fig. 7C). The LODs were calculated to be 7.4, 5.2 and 15.8 μmol/L for the Apple, Huawei and Xiaomi smartphones, respectively.

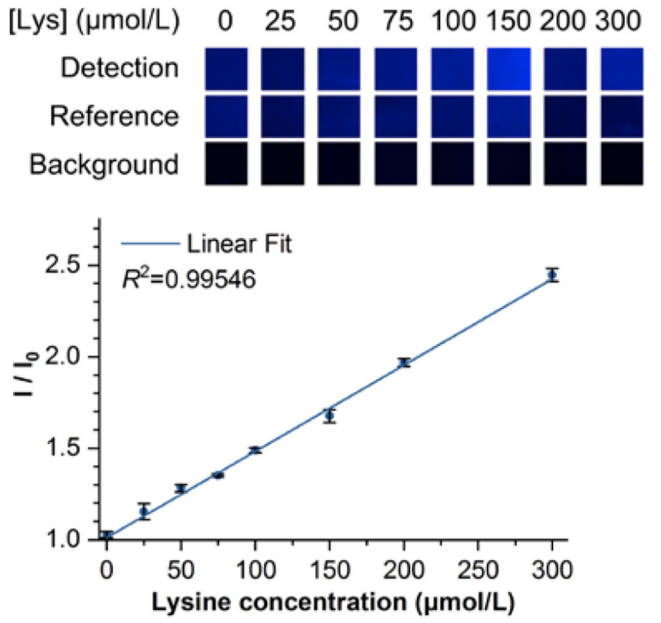


**Fig. 5.** Images captured by the inverted fluorescence microscope and the linear fitting curve of $I/I_0$ versus lysine concentration. $I/I_0$ = the relative light intensity.

### 3.5. Application in swine serum

To demonstrate its performance, the POCT platform was applied to a swine serum sample. As illustrated in Fig. 8, after collecting blood from a pig and centrifuging to obtain serum, only 3 steps are needed for lysine concentration determination: (1) add the serum sample into the detection channel of the microfluidic chip, (2) put the microfluidic chip into the box and take a photo with a smartphone, and (3) read the light intensity values and calculate the result using a predetermined equation.

Lysine concentration of the same swine serum sample was tested using different methods. The results of fluorescence assays using the developed N-CDs, including fluorescence detection using a spectrofluorophotometer, microfluidic chip-based detection using a fluorescence microscope and POCT using smartphones, are listed in Table 1. The measurement results obtained by smartphone-based POCT devices were calculated according to the calibration equation obtained by the Apple smartphone. All of these results matched well to the result obtained by the amino acid analyzer which was 46.8 μmol/L.

## 4. Discussion

To achieve sensitive and specific lysine detection, the first step is to synthesize high-performing sensors. We chose CDs as fluorescence probes because of their unique optical properties. The fluorescence intensity of CDs may be enhanced by lysine due to surface passivation (Liu et al., 2012; Song et al., 2017). However, the quantum yield of CDs is often less than 10%, limiting their practical application, especially in trace detection (Qu et al., 2012). Inspired by Wei et al. (2020), we utilized $ZnCl_2$ as the pyrolysis-promoting agent to increase the quantum yield. We then further improved the optical properties of synthesized CDs by doping CDs with electron-rich nitrogen atoms, which provide fluorescence-enhancing effects and offer more active sites (Zhang et al., 2014). The resulting N-CDs have high fluorescence quantum yield (24.8%), good photostability, sensitivity and specificity to lysine with a linear detection range of 5 to 300 μmol/L and LOD of 1.7 μmol/L. The detection range covers the typical range of lysine concentration in swine serum.

Then, in order to simplify the process and reduce the sample consumption, the fluorescence assay was incorporated into a microfluidic chip. Experiments have demonstrated that the fluorescence intensity of the N-CDs is stable under UV irradiation for 60 min. The hydrogel curing requires only 15 s of UV exposure and will not affect the fluorescence properties of the N-CDs. Compared with microfluidic paper-based analytical devices (μPADs), another commonly used POCT device, using hydrogel microstructures entrapping N-CDs as sensing elements provides better color intensity and uniformity and thus higher detection accuracy (Evans et al., 2014; Yang et al., 2019). As the images may be affected by fluctuations in excitation light intensity and emission collection efficiency, a reference channel with the same hydrogel sensing elements was set close to the detection channel and the relative fluorescence intensity $I/I_0$ was used as an indicator. The measurement was first carried out using a standard laboratory fluorescence

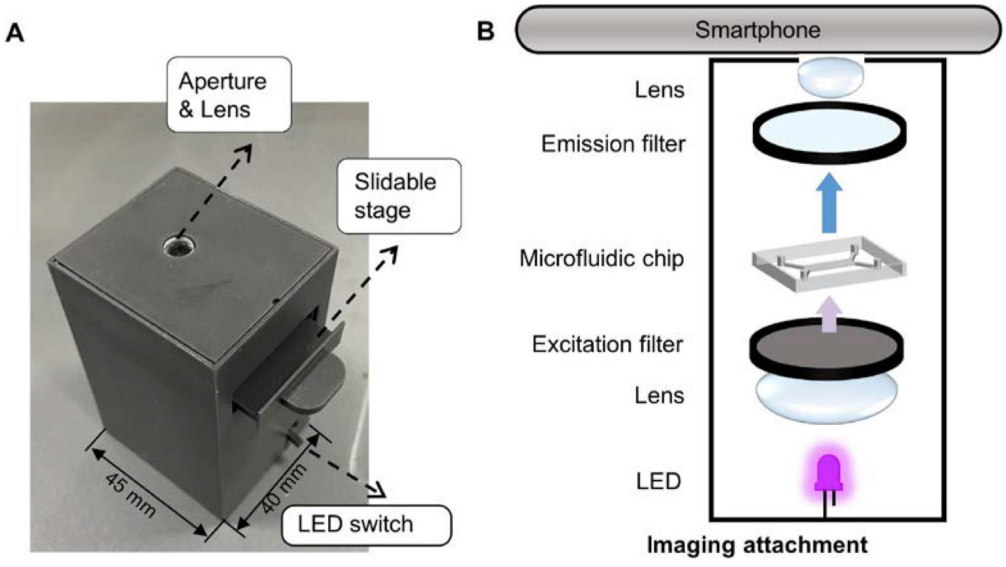


**Fig. 6.** The (A) photo and (B) schematic illustration of the imaging attachment to the phone.

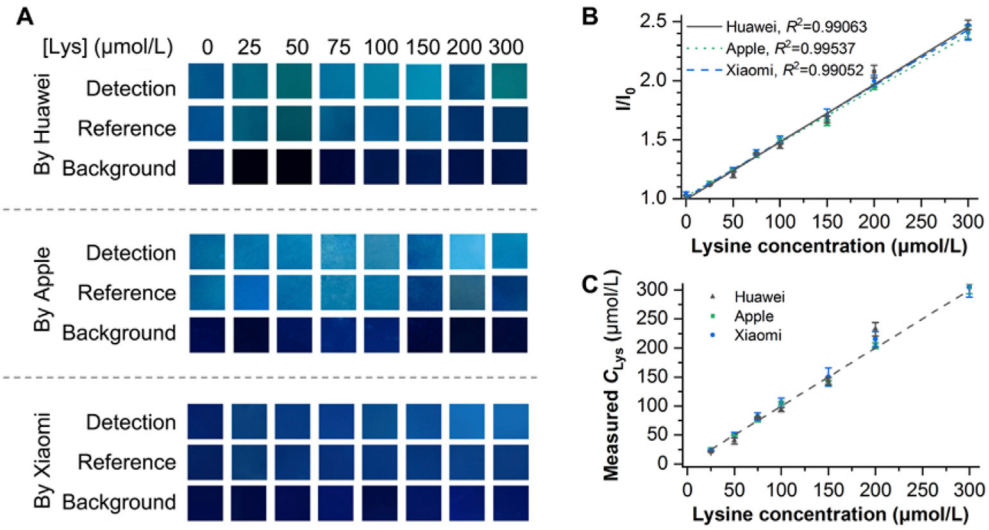


**Fig. 7.** The smartphone-based point-of-care testing (POCT) of lysine concentration. (A) Parts of the images captured by Huawei, Apple, and Xiaomi smartphones. (B) Linear fitting curves of the relative light intensity ($I/I_0$) versus the concentration of lysine. (C) Concentrations of lysine measured by Huawei, Apple, and Xiaomi smartphones versus the concentration of lysine, where the calibration equation obtained by the Apple smartphone was used. $C_{Lys}$ = the concentration of lysine.

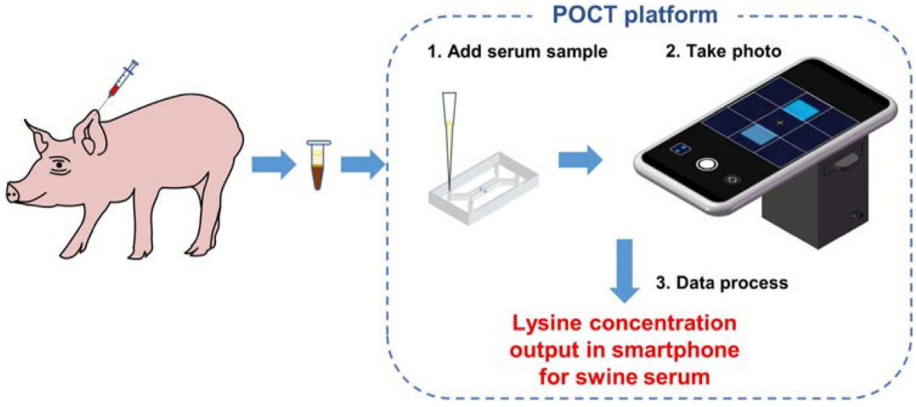


**Fig. 8.** Flowchart of the smartphone-based point-of-care testing (POCT) of lysine concentration.

**Table 1**
Lysine detection by different methods in swine serum.

| Methods | Detected concentration, μmol/L | RSD, % ($n = 3$) |
|---|---|---|
| Fluorescence spectra | 44.2 | 3.19 |
| Microfluidic chip-based POCT | | |
| Fluorescence microscope | 49.1 | 3.90 |
| Smartphone 1 (Huawei Nova 7 Pro) | 46.0 | 6.57 |
| Smartphone 2 (Apple iPhone 11) | 47.9 | 2.05 |
| Smartphone 3 (Xiaomi Mi 10S) | 44.4 | 4.56 |
| Amino acid analyzer | 46.8 | |

POCT = point-of-care testing; RSD = relative standard deviation.

microscope. Experimental results demonstrated that it is feasible to use a fluorescence microscope for lysine determination with high accuracy.

Finally, in order to use smartphones as an alternative to benchtop microscopes, an imaging attachment was designed to block light from the surrounding environment, providing a stable excitation illumination, and keeping a uniform relative positioning between the microfluidic chip and the smartphone. Current smartphone built-in cameras are not designed for precise analytical measurements. The integrated auto white balance function in smartphones, which decides the relative ratio of RGB signals, differs across smartphone brands and models leading to inconsistent colors of photos taken by different cameras for the same scene (Kong et al., 2019). Fortunately, in this work, it is the relative light intensity $I/I_0$, not the color information, which is used for calculations. The relative intensity $I/I_0$ for the same lysine concentration obtained by 3 smartphones from 3 popular brands was nearly identical and the same calibration equation could be used for the 3 smartphones. This suggests that POCT of lysine using different smartphones may be convenient, without requiring re-calibration each time and the smartphone-based imaging device may provide a universal portable platform to quantify the relative fluorescence intensity.

In summary, by synthesizing the N-CDs as lysine probes, fabricating the microfluidic chips, and designing a smartphone-based fluorescence imaging box, we have created a POCT platform for lysine determination. This platform requires only 3 μL serum sample and the testing can be done within 3 min. The conventional analysis of lysine mainly relies on HPLC (Dai et al., 2014; Regmi et al., 2016), which is limited by complicated sample pretreatment, time-consuming steps and high-cost instruments. The POCT platform can achieve consistent detection results with HPLC, while overcoming these disadvantages. However, HPLC can

simultaneously determine several different amino acid concentrations, which may be achieved by the POCT platform with various sensors added, but further studies are still needed.

The current POCT platform still has certain limitations. First, swine serum is needed. In future research, assays for whole blood could be developed by adding a plasma separation section to the microfluidic chip (Dimov et al., 2011; Yeh et al., 2017), which would eliminate the need for a centrifuge and further improve the testing speed. Second, a computer is needed for data processing. Although the light intensity in the captured image can be read by a smartphone app, such as Swatches (Guo et al., 2021), and then the results obtained manually using a calculator, the data processing is inconvenient. In future research, a smartphone app could be developed to enable automatic image and data processing and display the results with a user-friendly interface (Xu et al., 2020). Furthermore, the app could detect lysine nutrition deficiency or excess according to the test result and the pre-set upper and lower limits of normal values.

## 5. Conclusion

In summary, we developed a smartphone-based POCT platform for lysine determination using self-developed N-CDs as the fluorescence probe. The platform requires only 3 μL sample and 3 min to complete a test. It has been applied to swine serum samples and achieved high accuracy. It has the advantages of simple operation, rapid response, low cost, reduced blood collection volume and reduced swine stress. It may provide a rapid and portable platform for dynamic monitoring of swine lysine status and contribute to precise feed formula modulation with low-protein diet strategy.

## Author contributions

**Chizhu Ding:** Conceptualization, Methodology, Validation, Formal analysis, Investigation, Visualization, Writing original draft, Funding acquisition. **Xiang Chen:** Investigation, Validation, Formal analysis. **Xiaoyu Chen:** Investigation, Visualization. **Yue Liu:** Investigation, Validation. **Menglin Xia:** Investigation, Validation. **Ziyi He:** Conceptualization, Supervision, Project administration, Resources, Funding acquisition. **Qinshu Kang:** Investigation, Validation. **Xianghua Yan:** Conceptualization, Supervision, Project administration, Funding acquisition.

## Declaration of competing interest

We declare that we have no financial and personal relationships with other people or organizations that can inappropriately influence our work, and there is no professional or other personal interest of any nature or kind in any product, service and/or company that could be construed as influencing the content of this paper.

## Acknowledgments

We thank all Yan laboratory members for critical discussion and reading of the manuscript. This study was supported by the National Natural Science Foundation of China (32172782) to C.Z. Ding, and the National Natural Science Foundation of China (22104041) to Z.Y. He.

## References

Armstrong CW, McGregor NR, Sheedy JR, Buttfield I, Butt HL, Gooley PR. NMR metabolic profiling of serum identifies amino acid disturbances in chronic fatigue syndrome. Clin Chim Acta 2012;413(19–20):1525–31.

Baker SN, Baker GA. Luminescent carbon nanodots: emergent nanolights. Angew Chem Int Ed 2010;49(38):6726–44.

Chaicham C, Tuntulani T, Promarak V, Tomapatanaget B. Effective GQD/AuNPs nanosensors for selectively bifunctional detection of lysine and cysteine under different photophysical properties. Sens Actuators B Chem 2019;282:936–44.

Chen D, Wu W, Yuan Y, Zhou Y, Wan Z, Huang P. Intense multi-state visible absorption and full-color luminescence of nitrogen-doped carbon quantum dots for blue-light-excitable solid-state-lighting. J Mater Chem C 2016;4(38):9027–35.

Chen G, Chai HH, Yu L, Fang C. Smartphone supported backlight illumination and image acquisition for microfluidic-based point-of-care testing. Biomed Opt Express 2018;9(10):4604–12.

Culea M, Scrob S, Suvar S, Podea P, Haş I, Muste S. Determination of amino acids in corn seed by gas chromatography–mass spectrometry. Anal Lett 2015;48(1):37–46.

Dai Z, Wu Z, Jia S, Wu G. Analysis of amino acid composition in proteins of animal tissues and foods as pre-column o-phthaldialdehyde derivatives by HPLC with fluorescence detection. J Chromatogr B 2014;964:116–27.

Dimov IK, Basabe-Desmonts L, Garcia-Cordero JL, Ross BM, Ricco AJ, Lee LP. Stand-alone self-powered integrated microfluidic blood analysis system (SIMBAS). Lab Chip 2011;11(5):845–50.

Ettle T, Roth FX. Dietary selection for lysine by piglets at differing feeding regimen. Livest Sci 2009;122(2):259–63.

Evans E, Gabriel EFM, Coltro WKT, Garcia CD. Rational selection of substrates to improve color intensity and uniformity on microfluidic paper-based analytical devices. Analyst 2014;139(9):2127–32.

Guo L, Chen S, Yu YL, Wang JH. A smartphone optical device for point-of-care testing of glucose and cholesterol using Ag nps/uio-66-NH2-based ratiometric fluorescent probe. Anal Chem 2021;93(48):16240–7.

Jang E, Kim S, Koh WG. Microfluidic bioassay system based on microarrays of hydrogel sensing elements entrapping quantum dot–enzyme conjugates. Biosens Bioelectron 2012;31(1):529–36.

Ju J, Zhang R, He S, Chen W. Nitrogen-doped graphene quantum dots-based fluorescent probe for the sensitive turn-on detection of glutathione and its cellular imaging. RSC Adv 2014;4(94):52583–9.

Kong T, You JB, Zhang B, Nguyen B, Tarlan F, Jarvi K, et al. Accessory-free quantitative smartphone imaging of colorimetric paper-based assays. Lab Chip 2019;19(11):1991–9.

Lee S, Ibey BL, Coté GL, Pishko MV. Measurement of pH and dissolved oxygen within cell culture media using a hydrogel microarray sensor. Sens Actuators B Chem 2008;128(2):388–98.

Liao SF, Wang T, Regmi N. Lysine nutrition in swine and the related monogastric animals: muscle protein biosynthesis and beyond. SpringerPlus 2015;4(1):147.

Lin L, Gao Z, Wei H, Li H, Wang F, Lin JM. Fabrication of a gel particle array in a microfluidic device for bioassays of protein and glucose in human urine samples. Biomicrofluidics 2011;5(3):34112–3411210.

Liu JM, Lin Lp, Wang XX, Lin SQ, Cai WL, Zhang LH, et al. Highly selective and sensitive detection of Cu2+ with lysine enhancing bovine serum albumin modified-carbon dots fluorescent probe. Analyst 2012;137(11):2637–42.

Liu J, Geng Z, Fan Z, Liu J, Chen H. Point-of-care testing based on smartphone: the current state-of-the-art (2017–2018). Biosens Bioelectron 2019;132:17–37.

Long P, Feng Y, Cao C, Li Y, Han J, Li S, et al. Self-protective room-temperature phosphorescence of fluorine and nitrogen codoped carbon dots. Adv Funct Mater 2018;28(37):1800791.

Morbioli GG, Mazzu-Nascimento T, Stockton AM, Carrilho E. Technical aspects and challenges of colorimetric detection with microfluidic paper-based analytical devices (μPADs) – a review. Anal Chim Acta 2017;970:1–22.

Qu S, Wang X, Lu Q, Liu X, Wang L. A biocompatible fluorescent ink based on water-soluble luminescent carbon nanodots. Angew Chem Int Ed 2012;51(49):12215–8.

Regmi N, Wang T, Crenshaw MA, Rude BJ, Wu G, Liao SF. Effects of dietary lysine levels on plasma free amino acid profile in late-stage finishing pigs. SpringerPlus 2016;5(1):888.

Roy N, Lapierre H, Bernier JF. Whole-body protein metabolism and plasma profiles of amino acids and hormones in growing barrows fed diets adequate or deficient in lysine. Can J Anim Sci 2000;80(4):585–95.

Sharma N, Yun K. Dual sensing of tetracycline and l-Lysine using green synthesized carbon dots from Nigella sativa seeds. Dyes Pigment 2020;182:108640.

Song W, Duan W, Liu Y, Ye Z, Chen Y, Chen H, et al. Ratiometric detection of intracellular lysine and pH with one-pot synthesized dual emissive carbon dots. Anal Chem 2017;89(24):13626–33.

Tu WJ, Chen H, He J. Application of LC-MS/MS analysis of plasma amino acids profiles in children with autism. J Clin Biochem Nutr 2012:12–45.

Wang J, Zhang P, Li CM, Li YF, Huang CZ. A highly selective and colorimetric assay of lysine by molecular-driven gold nanorods assembly. Biosens Bioelectron 2012;34(1):197–201.

Wang Y, Zhou J, Wang G, Cai S, Zeng X, Qiao S. Advances in low-protein diets for swine. J Anim Sci Biotechnol 2018;9(1):60.

Wei SM, Feng K, Li C, Xie N, Wang Y, Yang XL, et al. $ZnCl_2$ enabled synthesis of highly crystalline and emissive carbon dots with exceptional capability to generate $O_2^{\cdot-}$. Matter 2020;2(2):495–506.

Wiltafsky MK, Bartelt J, Relandeau C, Roth FX. Estimation of the optimum ratio of standardized ileal digestible isoleucine to lysine for eight-to twenty-five-kilogram pigs in diets containing spray-dried blood cells or corn gluten feed as a protein source. J Anim Sci 2009;87(8):2554–64.

Wu G, Meininger CJ, Knabe DA, Baze FW, Rhoads MJ. Arginine nutrition in development, health and disease. Curr Opin Clin Nutr Metab Care 2000;3(1):59–66.

Würth C, Grabolle M, Pauli J, Spieles M, Resch-Genger U. Relative and absolute determination of fluorescence quantum yields of transparent samples. Nat Protoc 2013;8(8):1535–50.
Xie Y, Dai L, Yang Y. Microfluidic technology and its application in the point-of-care testing field. Biosens Bioelectron X 2022;10:100109.
Xu H, Xia A, Wang D, Zhang Y, Deng S, Lu W, et al. An ultraportable and versatile point-of-care DNA testing platform. Sci Adv 2020;6(17):eaaz7445.
Xue Z, Xiong L, Rao H, Liu X, Lu X. A naked-eye liquid-phase colorimetric assay of simultaneous detect cysteine and lysine. Dyes Pigment 2019;160:151–8.
Yang N, Chen C, Wang P, Sun J, Mao H. Structure optimization method of microfluidic paper chip based on image grey-level statistics for chromogenic reaction. Chem Eng Process Process Intensif 2019;143:107627.
Yeh EC, Fu CC, Hu L, Thakur R, Feng J, Lee LP. Self-powered integrated microfluidic point-of-care low-cost enabling (SIMPLE) chip. Sci Adv 2017;3(3):e1501645.
Yin J, Li Y, Han H, Liu Z, Zeng X, Li T, et al. Long-term effects of lysine concentration on growth performance, intestinal microbiome, and metabolic profiles in a pig model. Food Funct 2018;9(8):4153–63.
Yin J, Li Y, Zhu X, Han H, Ren W, Chen S, et al. Effects of long-term protein restriction on meat quality, muscle amino acids, and amino acid transporters in pigs. J Agric Food Chem 2017;65(42):9297–304.
Yuan L, Niu Y, Li R, Zheng L, Wang Y, Liu M, et al. Molybdenum oxide quantum dots prepared via a one-step stirring strategy and their application as fluorescent probes for pyrophosphate sensing and efficient antibacterial materials. J Mater Chem B 2018;6(20):3240–5.
Zeng PL, Yan HC, Wang XQ, Zhang CM, Zhu C, Shu G, et al. Effects of dietary lysine levels on apparent nutrient digestibility and serum amino acid absorption mode in growing pigs. Asian Australas J Anim Sci 2013;26(7):1003–11.
Zhang H, Chen Y, Liang M, Xu L, Qi S, Chen H, et al. Solid-phase synthesis of highly fluorescent nitrogen-doped carbon dots for sensitive and selective probing ferric ions in living cells. Anal Chem 2014;86(19):9846–52.
Zhou Y, Yang Z, Xu M. Colorimetric detection of lysine using gold nanoparticles aggregation. Anal Methods 2012;4(9):2711–4.